

# Lawrence Berkeley National Laboratory

## LBL Publications

### Title

OPTICAL AND EPR INVESTIGATIONS OF Np IN SINGLE CRYSTALS OF ZrSiO<sub>4</sub>

### Permalink

<https://escholarship.org/uc/item/0mk0g7mm>

### Author

Poirot, I.

### Publication Date

1987-05-01

c.2



# Lawrence Berkeley Laboratory

UNIVERSITY OF CALIFORNIA

Materials & Chemical  
Sciences Division

LIBRARY  
JUN 26 1987  
DOCUMENTS SECTION

Submitted to Physical Review B

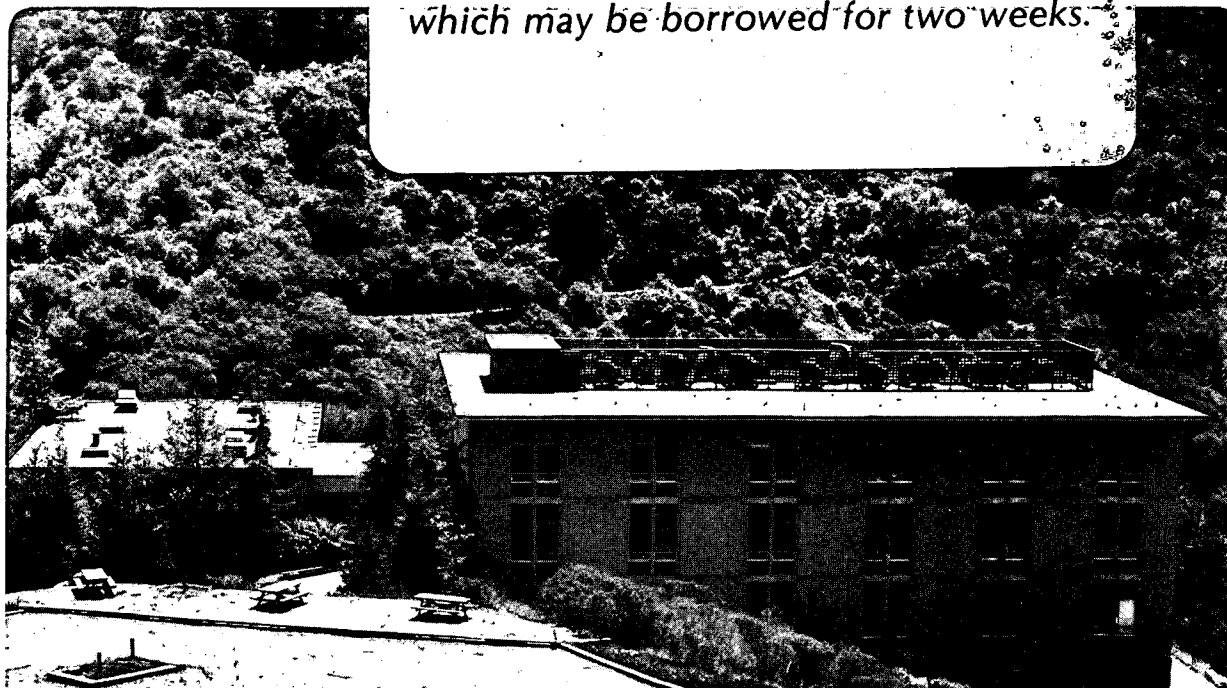
## OPTICAL AND EPR INVESTIGATIONS OF $Np^{4+}$ IN SINGLE CRYSTALS OF $ZrSiO_4$

I. Poirot, W. Kot, G. Shalimoff, N. Edelstein,  
M.M. Abraham, C.B. Finch, and L.A. Boatner

May 1987

**TWO-WEEK LOAN COPY**

*This is a Library Circulating Copy  
which may be borrowed for two weeks.*



LBL-23518  
c.2

## **DISCLAIMER**

This document was prepared as an account of work sponsored by the United States Government. While this document is believed to contain correct information, neither the United States Government nor any agency thereof, nor the Regents of the University of California, nor any of their employees, makes any warranty, express or implied, or assumes any legal responsibility for the accuracy, completeness, or usefulness of any information, apparatus, product, or process disclosed, or represents that its use would not infringe privately owned rights. Reference herein to any specific commercial product, process, or service by its trade name, trademark, manufacturer, or otherwise, does not necessarily constitute or imply its endorsement, recommendation, or favoring by the United States Government or any agency thereof, or the Regents of the University of California. The views and opinions of authors expressed herein do not necessarily state or reflect those of the United States Government or any agency thereof or the Regents of the University of California.

Optical and EPR Investigations of  $\text{Np}^{4+}$  in Single Crystals of  $\text{ZrSiO}_4$

I. Poirot, W. Kot, G. Shalimoff, N. Edelstein  
Materials and Chemical Sciences Division  
Lawrence Berkeley Laboratory  
and  
Department of Chemistry  
University of California  
Berkeley, California 94720

and

M.M. Abraham, C.B. Finch, L.A. Boatner  
Solid State Division  
Oak Ridge National Laboratory\*  
Oak Ridge, TN 37831

ABSTRACT

Polarized optical spectroscopy has been used to investigate the electronic structure of tetravalent neptunium incorporated as a dilute impurity in single crystals of the tetragonal host  $\text{ZrSiO}_4$ . Thirty-one levels were assigned from 30 intense polarized optical transitions and used in obtaining a fit to a parametric Hamiltonian to within an rms deviation of  $34 \text{ cm}^{-1}$ . Thirteen other levels with comparable intensities and good polarization characteristics were observed. An inclusion of these levels using the parameters from the 31 level fit, however, resulted in an increase of the rms deviation to approximately  $100 \text{ cm}^{-1}$ .

---

\* Operated by Martin Marietta Energy Systems, Inc. for the U.S.

Department of Energy under contract DE-AC05-84OR21400.

The EPR spectra of the ground state of  $\text{Np}^{4+}:\text{ZrSiO}_4$  were measured and fit to an axial spin Hamiltonian to obtain the parameters:  $|g_{\parallel}| = 0.8 \pm 0.6$ ,  $|g_{\perp}| = 2.59 \pm 0.02$ ,  $A = -2400 \pm 1200$  MHz, and  $B = 4750 \pm 30$  MHz. These results are consistent with the calculated  $\Gamma_6$  ground state.

## I. Introduction

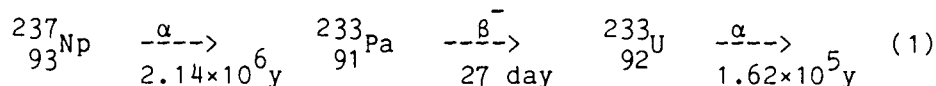
Investigations of the optical spectra of tetravalent neptunium incorporated as a dilute impurity in the single crystal hosts  $\text{ThO}_2$  and  $\text{PbMoO}_4$  were first reported in 1969.<sup>1,2</sup> Subsequently, optical spectroscopic studies of  $\text{Np}^{4+}$  in the host single crystal  $\text{CsNpCl}_6$  were carried out.<sup>3</sup> In all of these early investigations, assignments were only made to the low-lying levels of  $\text{Np}^{4+}$ . More recently, optical spectroscopic investigations of  $\text{Np}^{4+}$  doped into two additional host single crystals have been reported.<sup>4,5</sup> Tetravalent neptunium has been studied as a dilute impurity in  $\text{Zr}(\text{BD}_4)_4$  and 46 levels were assigned in the spectrum and fit to a parametric Hamiltonian with an rms deviation  $\sigma = 84 \text{ cm}^{-1}$ .<sup>4</sup>  $\text{Np}^{4+}$  has also been investigated as an impurity in single crystals of the zircon structure host  $\text{ThSiO}_4$ . In this case, 29 levels were assigned in the observed spectrum and these levels were fit with an rms deviation  $\sigma = 47 \text{ cm}^{-1}$ .<sup>5</sup> In the present work, optical spectroscopy has been used to investigate  $\text{Np}^{4+}$  in single crystals of  $\text{ZrSiO}_4$ . The observed optical transitions were assigned and used in obtaining fits to a parametric Hamiltonian. Additionally, Electron Paramagnetic Resonance (EPR) spectroscopy has been used to study the  $\text{Np}^{4+}$  ground state in zirconium silicate.

## II. Experimental

### A. Optical Measurements

Single crystals of  $\text{ZrSiO}_4$  doped with  $\text{Np}^{4+}$  were grown in platinum crucibles in air using a  $\text{Li}_2\text{O} \cdot 0.6\text{MoO}_3$  flux. After heating the crystal growth charge to  $1350^\circ\text{C}$ , the growth furnace was slowly cooled (at about  $1^\circ\text{C}/\text{h}$ ) to  $950^\circ\text{C}$ . The crystal growth procedures have been described in detail elsewhere.<sup>6-8</sup> Crystal growth runs were carried out with doping levels of 0.2 wt.% Np and 2.0 wt.% Np relative to  $\text{ZrSiO}_4$ . Single crystals of  $\text{ZrSiO}_4$  grown with the lower Np doping were well formed and transparent, and a specimen  $\sim 2 \times 2 \times 2 \text{ mm}^3$  was selected for use in the optical spectroscopic investigations. In the case of the  $\text{ZrSiO}_4$  crystals with the higher neptunium doping, although the crystals were larger relative to the lightly doped samples, they exhibited a green color and contained inclusions. Accordingly, it was necessary to prepare the optical samples by cutting thin ( $\sim 0.5 \text{ mm}$ ) sections with known orientations from the larger "as grown" crystals. The two types of crystals were mounted on slotted copper plates with their optical axis either perpendicular or parallel to the slit, and then sealed in quartz tubes containing a partial pressure of helium gas.

The Np concentration for both doping levels was determined by  $\gamma$ -ray counting methods. The Np decay (Eq. 1)



was at equilibrium in these crystals, and the relative intensities of the spectra of multiple  $\gamma$  and x-ray lines of Pa, U, and Np were compared to a reference with the same geometry (i.e., 1 mg of dissolved Np

evaporated on a copper plate and sealed in glass tubing). The high energy (100 to 340 keV)  $\gamma$  and x-ray lines of  $^{233}\text{Pa}$ , which were unaffected by the glass tubing and the crystal, gave measured Np concentrations of approximately 0.1 and 1.0 wt.% for the low and high doping levels of Np in  $\text{ZrSiO}_4$ , respectively.

The optical absorption spectra for both  $\sigma$  and  $\pi$  polarizations were recorded between 20000Å and 3500Å at room, liquid  $\text{N}_2$ , and liquid He temperatures (see Figs. 1 and 2) using a Cary 17 spectrophotometer. In addition, absorption spectra in the 7600-3500Å range were taken at 4.2K with Jarrell-Ash F6 and 3.4 m-spectrographs. At liquid helium temperature, the observed line widths varied between 15 and 70  $\text{cm}^{-1}$ , with the average value being approximately 30  $\text{cm}^{-1}$ . Attempts were made to obtain the Zeeman spectra in a magnetic field of 2.7 T at 4.2K with the magnetic field applied parallel and perpendicular to the optical axis, but no line broadening or splittings were observed. Additionally, no fluorescence was observed in the visible and near IR regions and no electronic Raman spectra were detected at 4.2K for either crystal.

#### B. EPR Measurements

EPR spectra were obtained at 4.2K and 35 GHz using a Varian E110 microwave resonance spectrometer with an electromagnet that could be rotated about the vertical axis. The maximum obtainable magnetic field was 16 kG. The magnetic-field positions of the EPR transitions were measured by proton NMR, and the microwave frequency was determined with an EIP frequency counter.

A single crystal of Np doped  $\text{ZrSiO}_4$  was selected and oriented in the cylindrical 35 GHz cavity ( $\text{TE}_{011}$ ) so that the applied magnetic field

could be rotated in the ac crystallographic plane. All six hyperfine lines for the  $I=5/2$   $^{237}\text{Np}$  isotope were observed with  $\vec{H}$  perpendicular to the c-axis of the crystal. These lines moved to higher field values as the field orientation was rotated toward the crystal c-axis. Magnetic-field positions were recorded as a function of the magnetic-field orientation at angles where at least three hyperfine lines could be observed (the other lines having shifted above the range of the magnetic field). This corresponded to a rotation of approximately  $\pm 50^\circ$  about the direction perpendicular to the c-axis. Additionally, because of problems in positioning the crystal that was encapsulated in polyethylene tubing in the microwave cavity, a  $\pm 10^\circ$  uncertainty is estimated in the orientation of the plane of magnetic-field rotation relative to the ac plane of the  $\text{ZrSiO}_4$  crystal.

### III. Optical Results

The optical absorption results obtained as described in Sec. II-A above can be divided into six groups of transitions. Table I lists the wavelengths for the transitions observed with both the dilute and concentrated  $\text{Np}^{4+}$  doped  $\text{ZrSiO}_4$  single crystals along with the polarization characteristics, intensities, and assignments for the transitions. The features and details of the six groups of optical transitions are described in the following section.

#### A. First Group (5000-6000 $\text{cm}^{-1}$ ; 20000-15000Å)(Fig. 1)

Six absorption bands appeared in this range in  $\text{ZrSiO}_4$  crystals with both  $\text{Np}^{4+}$  doping levels. These features became better resolved as the crystals were cooled. Five of the bands showed strong  $\sigma$  or  $\pi$



polarization and could be assigned to transitions from a  $\Gamma_6$  ground state to a higher lying  $\Gamma_6$  or  $\Gamma_7$  level based on the polarization characteristics. Only a few of the bands exhibited the expected polarization extinction. Generally, the  $\pi$  absorption lines were not accompanied by a  $\sigma$  transition (at 5514, 6072, 6096  $\text{cm}^{-1}$ ) as permitted by the selection rules. This clearly isolated group was assigned to the  $^4I_{11/2}$  multiplet. Six stark levels, three  $\Gamma_6$  and three  $\Gamma_7$ , result from the crystal field interaction. The  $17470 \pm 10\text{A}$  band must be attributed to a transition to a  $\Gamma_6$  level even though a very weak and broad absorption appears with  $\pi$  polarization.

The weak, broad absorption at about 19350A was only observed at room temperature and gave an indication of the ground term splitting. This peak is separated by 350  $\text{cm}^{-1}$  from the 5515  $\text{cm}^{-1}$  transition. It has the same  $\pi$  polarization and resulted from the partial population of the first excited  $\Gamma_6$  level of the  $^4I_{9/2}$  manifold at room temperature.

Some other broad, weak lines and shoulders were observed, but they could not be assigned. These features may be due to electronic plus vibronic excitations. Furthermore, particularly in this group, the heavily doped  $\text{ZrSiO}_4$  crystal showed additional absorption lines as compared to the more dilute crystal. These extra lines were strongly polarized and indicate that an additional site may be present at higher Np concentration levels.

#### B. Second Group (8300-8400 $\text{cm}^{-1}$ , 12500-11500A)(Fig. 1)

Two absorption lines are observed in this range and these were assigned to the  $^4F_{3/2}$  state that is split into  $\Gamma_6$  and  $\Gamma_7$  levels. Again the  $\Gamma_6$  to  $\Gamma_7$  transition is intense for  $\pi$  polarization (at 12000A) for

both Np concentrations, but is very weak in  $\sigma$  polarization, and in fact, is barely visible in the dilute Np-doped crystal.

C. Third Group (9600-12600  $\text{cm}^{-1}$ , 10500-7900Å)(Fig. 1)

According to preliminary calculations (See Sec. IV-A), the  $J = 13/2$ ,  $9/2$  (II) and  $5/2$  (I) manifolds are expected to be found in this group. At this point, however, it was difficult to classify the individual  $J$  states for the 14 absorption bands detected in this range. Nine lines in this region could be identified as  $\Gamma_6$  or  $\Gamma_7$  crystal field levels according to their polarization characteristics. As in the case of the first group, a weak, broad line at  $9660 \text{ cm}^{-1}$  was found about  $350 \text{ cm}^{-1}$  from the next intense transition, and this line was detected only at room temperature. This temperature-dependent line confirmed the assignment of the first excited state at  $350 \text{ cm}^{-1}$ .

D. Fourth Group (13200-16085  $\text{cm}^{-1}$ , 7800-6100Å)(Fig. 2)

A difference of only  $650 \text{ cm}^{-1}$  separated this group from the third group of transitions. Because of  $J$  mixing by the crystal field, some overlap may occur between this group and the lower energy one. Nevertheless, assuming that the  $J$  levels are relatively isolated, levels derived from the  $J = 5/2$ (II),  $3/2$ (II),  $7/2$ (I), and  $15/2$ (I) are expected. Nine of the observed 14 bands in this group could be assigned from their polarization characteristics.

E. Fifth Group (16495-16640  $\text{cm}^{-1}$ , ~6000Å)(Fig. 2)

Only two transitions appeared in this group that were separated from the other groups. As in other compounds of  $\text{Np}^{4+}$ , these transitions

can be attributed to the  ${}^4G_{7/2}$  manifold. One transition is strongly  $\pi$  polarized ( $\Gamma_7$ ) and the other is strongly  $\sigma$  polarized ( $\Gamma_6$ ).

F. Sixth Group (17600-28800  $\text{cm}^{-1}$ , 5800-3500Å)(Fig. 2)

This group represents the highest energy part of the spectrum, and it was relatively complex. Fourteen intense lines could be identified as  $\Gamma_6$  or  $\Gamma_7$ , however, from their strongly polarized transitions.

#### IV. Optical Data Analysis

##### A. Energy Level Assignments

The energy levels within an  $f^n$  configuration in  $D_{2d}$  symmetry can be written in terms of the free-ion ( $H_{FI}$ ) and crystal-field ( $H_{CF}$ ) Hamiltonians as follows:<sup>9-11</sup>

$$H_{FI} = \sum_{k=0,2,4,6} F^k(nf,nf)f_k + \zeta_f a_{so} + \alpha L(L+1) \quad (2)$$

$$+ BG(G_2) + \gamma(R_7) + \sum_{k=0,2,4} M^k m_k + \sum_{2,4,6} P^k p_k$$

and

$$H_{CF} = B_0^2 C_0^2 + B_0^4 C_0^4 + B_4^4 (C_4^4 + C_{-4}^4) \quad (3)$$

$$+ B_0^6 C_0^6 + B_4^6 (C_4^6 + C_{-4}^6).$$

The  $F^k(nf,nf)$ 's and  $\zeta_f$  above represent the radial parts of the electrostatic and spin-orbit interactions, respectively, between  $f$  electrons, while  $f_k$  and  $a_{so}$  are angular parts of these interactions.

The parameters  $\alpha$ ,  $\beta$ , and  $\gamma$  are associated with the two-body effective operators of the configuration interaction. The  $M^k$  parameters represent the spin-spin and spin-other-orbit interactions while the  $P^k$  parameters arise from electrostatic-spin-orbit interactions with higher configurations. The crystal field interaction for  $D_{2d}$  symmetry is parameterized by  $B_0^2$ ,  $B_0^4$ ,  $B_4^4$ ,  $B_0^6$ , and  $B_4^6$ , and the angular operators  $C_q^{(k)}$  are the usual Racah tensors.

For an odd number of electrons (as in  $Np^{4+}$ ,  $5f^3$ ) in  $D_{2d}$  symmetry, the Kramers degenerate states are classified by the  $\Gamma_6$  and  $\Gamma_7$  double group representations. The selection rules for the allowed electric-dipole transitions in this symmetry are given in Table II. In  $ZrSiO_4$  crystals containing  $Np^{4+}$  at both doping levels, the absorption spectra did not precisely follow the expected polarization. This effect will be described more fully later.

The optical spectra of  $U^{4+}$  doped into both  $ZrSiO_4$  and  $ThSiO_4$  single crystals have previously been studied.<sup>12-14</sup> Although these two host crystals are isostructural as noted above, the size of the positive metal ions  $Zr^{4+}$  and  $Th^{4+}$  is quite different. This size difference results in a crystal field whose strength is very different for the two crystals at the site of an impurity ion such as  $U^{4+}$  or  $Np^{4+}$ . Accordingly, the spectra of  $U^{4+}:ThSiO_4$  and  $U^{4+}:ZrSiO_4$  differ quite markedly. (It is interesting to note that the resemblance of the spectrum of  $U^{4+}:ThSiO_4$  to that of  $U^{4+}:ThBr_4$  has recently led to a reanalysis of the data for these systems.<sup>14</sup>) Nevertheless it is expected that the crystal-field parameters will not vary greatly for two consecutive ions in the periodic table (the only difference being in the number of f electrons) in the same host crystal. This premise is

exploited in carrying out the analysis of the optical spectrum of  $\text{Np}^{4+}:\text{ZrSiO}_4$  in the present work.

A preliminary calculation was performed using the free-ion parameters obtained from the analysis of the optical results of either  $\text{Np}^{4+}:\text{Zr}(\text{BD}_4)_4$  or  $\text{Np}^{4+}:\text{ThSiO}_4$  along with the crystal-field parameters obtained from the analysis of the data for  $\text{U}^{4+}:\text{ZrSiO}_4$ . These calculations predicted a  $\Gamma_6$  ground state that is well separated from the higher energy levels as well as relatively isolated J levels for those whose energy was less than  $-10000 \text{ cm}^{-1}$ .

#### B. Parametric Fit of the Optical Data

From the calculated energy levels, 30 transitions could be assigned for which there was good agreement between the calculated and measured energies along with consistency for the polarization characteristics and with the expected eigenvector composition. The free-ion parameters  $F^2$ ,  $F^4$ ,  $F^6$ , and  $\zeta$  were varied with the crystal-field parameters fixed at the  $\text{U}^{4+}:\text{ZrSiO}_4$  values. The crystal-field parameters were then allowed to vary with the free-ion parameters fixed, and finally, all of the above parameters were varied simultaneously. The remaining parameters were fixed at the values used for  $\text{Np}^{4+}:\text{Zr}(\text{BD}_4)_4$ . For the fit with 31 levels, an rms deviation of  $34 \text{ cm}^{-1}$  was obtained.

Thirteen additional transitions were present that, together with the 30 transitions discussed above, correspond to the strongest observed transitions. The addition of these 13 transitions resulted in some interchanges in the  $\Gamma_6$  and  $\Gamma_7$  levels in the calculated spectrum. Furthermore, fitting these additional levels did not significantly improve the rms deviation obtained by using the parameters resulting

from the 31 level fit when the extra 13 transitions were assigned to the nearest calculated energy level of the correct symmetry.

The final values of the parameters obtained with the 31 level fit are given in Table V and this fit resulted in an rms deviation of  $\sigma = 34 \text{ cm}^{-1}$  as noted above (varying 12 parameters including  $\alpha$  and  $\beta$ ). For the fit with 44 levels a value for  $\sigma$  of  $103 \text{ cm}^{-1}$  was obtained. The calculated energy levels and eigenvectors are given in Table VI.

#### V. EPR Ground State Data and Analysis

The EPR line positions obtained as a function of the applied magnetic-field orientation were fitted to the parameters of the axial spin-Hamiltonian<sup>15</sup>

$$\begin{aligned} \mathcal{H} = & g_{\parallel} \mu_B H_z S_z + g_{\perp} \mu_B (H_x S_x + H_y S_y) \\ & + A_{\parallel} S_z I_z + A_{\perp} (S_x I_x + S_y I_y) \end{aligned} \quad (4)$$

where  $\mu_B$  is the Bohr magneton and H is the magnetic field. The other parameters have their usual meaning. Due to the small value of  $g_{\parallel}$  and the problems with the orientation of the crystal, the uncertainties in the values of  $g_{\parallel}$  and A are much greater than the errors in  $g_{\perp}$  and B. The resulting parameters for the spin-Hamiltonian are given in Table III. An additional analysis was attempted in which a quadrupolar term was added to the spin-Hamiltonian, but this refinement did not significantly improve the fit. The data given in Table III are consistent with the calculated  $\Gamma_6$  calculated ground state and serve to confirm that assignment.

For a pure  $J$  state, the ratio of  $a/g$ ,  $A/g_{||}$ , and  $B/g_{\perp}$  should be constant, (where  $a$  and  $g$  are, respectively, the hyperfine coupling constant and  $g$  value of a particular  $J$  manifold of the free ion). There are two other reported measurements for  $\text{Np}^{4+}$  in various crystals or molecules,<sup>4,16</sup> and these ratios are given in Table IV along with the present value obtained for  $\text{Np}^{4+}$  in  $\text{ZrSiO}_4$ . The ground state wavefunction obtained from the optical fit shows that the ground state is -97% pure  $J = 9/2$ . Therefore, this ratio should represent a check on the validity of the present data. The agreement between the earlier  $a/g$  ratios and the  $B/g_{\perp}$  value obtained in this work are considered to be satisfactory. The experimental uncertainties in  $A$  and  $g_{||}$ , however, are too great to apply this test.

## VI. Discussion

The zircon structure is representative of a class of tetragonal crystals that includes  $\text{ThSiO}_4$ ,  $\text{HfSiO}_4$ ,  $\text{ZrSiO}_4$ ,  $\text{YPO}_4$  and the heavier lanthanide ortho phosphates, vanadates, and arsenates. The metal ion is located at a site of  $D_{2d}$  symmetry surrounded by eight oxygen atoms in a dodecahedral array. The  $S_4$  axis of the metal atom site is parallel to the optic axis of the crystal.<sup>17-19</sup>  $\text{Zr}^{4+}$  has an eight-coordinate ionic radius of 0.84Å while the eight-coordinated ionic radius of  $\text{Th}^{4+}$  is 1.05Å.<sup>20</sup> Thus, when a  $\text{Np}^{4+}$  ion substitutes for a  $\text{Zr}^{4+}$  ion, a movement of the surrounding atoms away from the impurity ion is expected. For  $\text{ThSiO}_4$ , however, the  $\text{Np}^{4+}$  impurity ion should cause much less distortion. Furthermore, the crystal-field interaction experienced by the  $\text{Np}^{4+}$  ion will be larger in  $\text{ZrSiO}_4$  than in  $\text{ThSiO}_4$ .

Table VII lists the parameters for those actinide ions in  $\text{ZrSiO}_4$  and  $\text{ThSiO}_4$  whose optical spectra have been analyzed. It is reassuring to note that the crystal-field parameters for  $\text{U}^{4+}:\text{ZrSiO}_4$  and  $\text{Np}^{4+}:\text{ZrSiO}_4$  are very similar. The crystal-field parameters for  $\text{Np}^{4+}:\text{ZrSiO}_4$  are quite different and much larger than those for  $\text{Np}^{4+}:\text{ThSiO}_4$ . This is indicative of the much larger crystal field found in the  $\text{ZrSiO}_4$  host as shown qualitatively by the Auzel parameter<sup>21</sup>  $N_V/(4\pi)^{1/2}$  that is also listed in Table VII.

For  $f^n$  ions where  $n$  is odd, the selection rules are not very restrictive. The present analysis is essentially based on crystal-field parameters obtained from the  $\text{U}^{4+}:\text{ZrSiO}_4$  analysis. With the use of these parameters and the  $\text{Np}^{4+}$  free-ion parameters resulting from the  $\text{Np}^{4+}:\text{Zr}(\text{BD}_4)_4$  analysis, it was possible to assign 31  $\text{Np}^{4+}$  energy levels rather easily, and adjustment of the parameters as described earlier led to a very good value for  $\sigma$ . It is rather disturbing, however, that 13 other transitions of comparable intensity and with good polarization characteristics led to an increased rms deviation of  $\sim 100 \text{ cm}^{-1}$ . A number of fits were attempted with various starting parameters, but these resulted in the inversion of several  $\Gamma_6$  and  $\Gamma_7$  levels without producing a significant decrease in  $\sigma$ . The resulting parameters from the 31 level fit, however, were used to calculate the rms deviation for all of the observed strong transitions.

The reason for the above discrepancy is not understood at present. The absorption lines were very broad, and the line width did not decrease markedly in the dilute crystal. It is possible that more than one Np site is present in these crystals that could be responsible for the observed large line widths and the noted marked deviations in the



fit for some levels. Additionally, impurities can arise from the flux used in the crystal growth process. Unfortunately, however, it is difficult to explore a variety of growth conditions when radioactive materials are employed.

Although the free-ion parameters for  $\text{Np}^{4+}:\text{ZrSiO}_4$  were obtained over a small energy range and must be considered to be rather tentative, the ratios of the parameters given in Table VII, that have been defined by Rajnak et al.,<sup>4</sup> are consistent with the observations in that work. All of the  $\text{Np}^{4+}:\text{ZrSiO}_4$  ratios indicate decreasing covalency with increasing atomic number as compared to the results for  $\text{U}^{4+}$  in  $\text{ZrSiO}_4$ . It should be noted, however, that there is increased scatter when the corresponding ratios are compared for  $\text{U}^{4+}$  and  $\text{Np}^{4+}$  in the  $\text{ThSiO}_4$  host.

## VII. Conclusion

The optical spectrum of  $\text{Np}^{4+}:\text{ZrSiO}_4$  has been analyzed with 31 strong transitions assigned using crystal-field parameters consistent with those determined previously for  $\text{U}^{4+}:\text{ZrSiO}_4$ . Thirteen other relatively intense levels did not fit well. EPR results confirmed the assignment of the ground crystal-field state of  $\text{Np}^{4+}$  in  $\text{ZrSiO}_4$ . A comparison of the empirical parameters obtained for  $\text{Np}^{4+}:\text{ZrSiO}_4$  with those obtained for the  $\text{U}^{4+}:\text{ZrSiO}_4$  shows the same trends as those found in comparing the parameters of  $\text{Np}^{4+}:\text{Zr}(\text{BD}_4)_4$  with those of  $\text{U}^{4+}:\text{Hf}(\text{BD}_4)_4$ <sup>4,22</sup> i.e., covalency effects are found to decrease with increasing atomic number.

Acknowledgement

This work was supported by the Director, Office of Energy Research, Office of Basic Energy Sciences, Chemical Sciences Division of the U.S. Department of Energy under Contract No. DE-AC03-76SF00098 and by the Division of Materials Science, U.S. Department of Energy, under Contract No. DE-AC05-84OR21400 with Martin Marietta Energy Systems, Inc.

We wish to thank Ray Gatti for help with the gamma counting experiments and Glen Williams for running the electronic Raman experiment and Homer Harmon for his technical assistance during the growth of these radioactive materials. The authors are also indebted to John Bigelow and other staff members of the transuranium element production facilities at the Oak Ridge National Laboratory.

## References

- [1] J.B. Gruber and E.R. Menzel, *J. Chem. Phys.* 50, 3772 (1969).
- [2] K.K. Sharma and J.O. Ortman, *J. Chem. Phys.* 50, 1241 (1969).
- [3] E.R. Menzel and J.B. Gruber, *J. Chem. Phys.* 54, 3857 (1971).
- [4] K. Rajnak, R.H. Banks, E. Gamp, and N. Edelstein, *J. Chem. Phys.* 80, 5951 (1984).
- [5] M.P. Lahalle, J.C. Krupa, and R. Guillaumont, *J. Less-Common Metals* 122, 65 (1986).
- [6] A.A. Ballman and R.A. Laudise, *J. Amer. Ceram. Soc.* 48, 130 (1965).
- [7] A.B. Chase and J.A. Osmer, *J. Electrochem. Soc.* 113, 198 (1966).
- [8] D. Ball and B.M. Wanklyn, *Phys. Stat. Sol. (a)* 36, 307 (1976).
- [9] B.G. Wybourne, "Spectroscopic Properties of the Rare Earths," (Wiley & Sons, New York, 1965).
- [10] B.R. Judd, "Operator Techniques in Atomic Spectroscopy," (McGraw Hill, New York, 1963).
- [11] W.T. Carnall, H. Crosswhite, and H.M. Crosswhite, J.P. Henla, N.M. Edelstein, J.G. Conway, G.V. Shalimoff, and R. Sarup, *J. Chem. Phys.* 72, 5089 (1980).
- [12] D.J. Mackey, W.A. Runciman, and E.R. Vance, *Phys. Rev. B* 11, 211 (1975).
- [13] E.R. Vance, D.J. Mackey, *Phys. Rev. B* 18, 185 (1978).
- [14] C. Khan Malek, J.C. Krupa, P. Delamoye, and M. Genet, *J. Less-Common Metals* 122, 75 (1986).
- [15] A. Abragam and B. Bleaney, "Electron Paramagnetic Resonance of Transition Ions," Clarendon Press, Oxford, 1970.
- [16] N. Edelstein, W. Kolbe, and J.E. Bray, *Phys. Rev. B* 21, 338 (1980).

- [17] R.W. Wyckoff, "Crystal Structures," 2nd Ed. Interscience, New York, 1965, Vol. 3, pp. 15.
- [18] R.W. Reynolds, L.A. Boatner, C.B. Finch, A. Chatelain, and M.M. Abraham, J. Chem. Phys. 56, 5607 (1972).
- [19] Vishwamittar and S.P. Puri, Phys. Rev. B 9, 4673 (1974).
- [20] R.D. Shannon, Acta Cryst. A 32, 751 (1976).
- [21] F. Auzel and O.L. Malta, J. Phys. (Paris) 44, 201 (1983).
- [22] K. Rajnak, E. Gamp, R. Shinomoto, and N. Edelstein, J. Chem. Phys. 80, 5942 (1984).

Table I. Absorption spectra of  $\text{Np}^{4+}/\text{ZrSiO}_4$ 

$\lambda(\text{\AA})$ Conc. crystal	$\lambda(\text{\AA})$ Diluted crystal	Energy ( $\text{cm}^{-1}$ )	Polarization	Intensity	Assigned Representation
1st Group					
19348	19350	5167	$\pi$	W(dis. at 4K)	
19079	19150	5240	$\sigma, \pi$	VW & Br.	
18131	18140	5514	$\pi$	S	$\Gamma_7$
18029		5545	$\pi$	vw	
17472	17472	5723	$\sigma, \pi$ weak	M	$\Gamma_6$
16692		5989	$\sigma$	M	
16506	16470	6056	$\sigma$	M	$\Gamma_6$
16465	16420	6072	$\pi$	M	$\Gamma_7$
15586	15520	6500	$\sigma, \pi$	sh.	
15456	15450	6468	$\sigma$	S	$\Gamma_6$
15391	15380	6496	$\pi$	VS	$\Gamma_7$
2nd Group					
12030	12000	8310	$\pi, \sigma$ weak	M	$\Gamma_7$
11950	11930	8366	$\sigma$	M	$\Gamma_6$
3rd Group					
10350	10350	9659	$\sigma$	vw(dis. at 4K)	
10175		9825	$\sigma, \pi$	vw & Br.	
9981	9960	10016	$\sigma$	W	$\Gamma_6$
9936	9920	10062	$\pi$	W	$\Gamma_7$
9634		10377	$\sigma, \pi$	sh.	
9566	9568	10450	$\sigma, \text{st.} \pi$	M	$\Gamma_7^*$
9237	9220	10823	$\sigma, \pi$	vw, sh.	
9175	9160	10896	$\sigma, \text{st.} \pi$	VS	$\Gamma_7^*$
8971	8969	11147	$\text{st.} \sigma, \pi$	VS	$\Gamma_6^*$
8880		11258	$\sigma$	sh.	
8640	8615	11571	$\sigma, \pi$ weak	S	$\Gamma_6^*$
8376	8350	11935	$\sigma, \pi$ weak	S	$\Gamma_6$
8197	8195	12196	$\sigma, \text{st.} \pi$	VS	$\Gamma_7$
7974	7930	12537	$\sigma, \pi$ weak	S	$\Gamma_6$
4th Group					
7590	7570	13188	$\sigma$	S	$\Gamma_6$
7495	7480	13352	$\pi$	S	$\Gamma_7$
7513		13306	$\sigma$	sh	
7243		13802	$\sigma$	vw	

7225	7200	13861	$\pi$	S	$\Gamma_7^*$
7135	7110	14036	$\sigma$	S	$\Gamma_6^*$
7061		14158	$\pi$	M	$\Gamma_7^*$
6904	6870	14555	$\pi$	S	$\Gamma_7$
6818		14663	$\sigma, \pi$ sh	W	
6664	6653	15014	$\sigma, \pi$	M	$\Gamma_7$
6511	6502	15365	$\sigma$	M	b
6444	6437	15514	$\sigma$	W	
6255	6250	15983	$\pi, \sigma$ sh	S	$\Gamma_7^*$
6240	6235	16025	$\sigma$	S	$\Gamma_6^*$

## 5th group

6064	6057	16495	$\pi$	M	$\Gamma_7$
6011	6005	16640	$\sigma$	S	$\Gamma_6^*$

## 6th Group

5681	5672	17610	$\sigma$	vw	
5630	5654	17750	$\sigma$	vw	
5595	5588	17869	$\sigma$	M	$\Gamma_6^*$
5509	5500	18160	$\sigma$	W	
5432	5427	18410	st. $\sigma, \pi$	VS	$\Gamma_6$
5396	5413	18500	$\sigma$	vw	
5370	5362	18630	$\sigma$	vw, sh.	
5343	5337	18720	$\sigma, \pi$	W	
5324		18780	$\sigma, \pi$	sh.	
5285		18916	$\pi$	vw	
5248	5250	19045	$\sigma, \pi$ weak	M	$\Gamma_6$
5168	5161	19350	$\sigma, \text{st.}\pi$	S	$\Gamma_7^*$
5137		19460	$\sigma$	vw	
5096	5090	19630	$\sigma, \pi$	S	$\Gamma_6^*$
5073	5066	19715	$\pi$	sh	
5030	5019	19895	$\pi$	M	$\Gamma_7$
5018	5014	19930	$\sigma$	S	$\Gamma_6$
4943	4939	20230	$\sigma$	M	
4885	4883	20470	$\sigma$	S	$\Gamma_6$
4859	4857	20580	$\sigma$	sh	
4822	4826	20730	$\pi$	W	
4815	4815	20762	$\sigma$	vw	
4752	4750	21038	$\pi$	M	
4743	one	21078	$\sigma$	vw	
4730	broad	21135	$\sigma$	sh.	
4683	line	21347	$\pi$	vw	
4601		21728	$\sigma$	M	$\Gamma_6$
4579	4592	21847	$\sigma, \pi$	S	$\Gamma_7$
4482	4479	22310	$\sigma, \pi$	vw	
4431	4429	22567	$\pi$	M	$\Gamma_7$
4424		22598	$\sigma$	vw	
4350	4343	22999	$\sigma$	VS	
4332	4323	23100	$\pi$	vw	$\Gamma_7$
4291	4284	23320	$\sigma$	S	b

4270		23413	$\sigma$	sh	
4210	4201	23760	$\pi, \sigma$ weak	W	$\Gamma_7$
4177	4170	23930	$\sigma, \pi$	M	$\Gamma_7$
4135		24177	$\sigma$	vw	
4092		24431	$\sigma$	vw	
3777	3769	24490	$\sigma$	M	
3759	3759	26595	$\sigma$	sh	
3530		28320	$\sigma$	W	
3474		28777	$\sigma$	W	

---

<sup>a</sup>VS, very strong; S, strong; M, medium; W, weak; vw, very weak;  
sh., shoulder

<sup>b</sup>These transitions were not assigned.

\*These transitions were assigned but not used in the fitting procedure.

Table II. Electric dipole selection rules for  $D_{2d}$  symmetry for an  $f^n$  ion ( $n$  odd)

	$\Gamma_6$	$\Gamma_7$
$\Gamma_6$	$\sigma$	$\sigma, \pi$
$\Gamma_7$	$\sigma, \pi$	$\sigma$



Table III. Spin-Hamiltonian parameters for  $\text{Np}^{4+}/\text{ZrSiO}_4$ 

---

	EPR	Optical*
$ g_{  } $	$0.8 \pm 0.6$	-0.1
$ g_{\perp} $	$2.59 \pm 0.02$	2.9
A(MHz)	$-2400 \pm 1200$	
B(MHz)	$4750 \pm 30$	

---

\* Calculated from the wavefunctions obtained from fitting the optical spectra.

Table IV. Ratios of the hyperfine coupling constants and g values.

Compound	$\frac{a}{g}$ or $\frac{B}{g} \perp$	Ref.
$\text{Np}^{4+}:\text{Cs}_2\text{ZrCl}_6$	$1848 \pm 60$	20
$\text{Np}(\text{BH}_4)_4:\text{Zr}(\text{BH}_4)_4$	1807	4
$\text{Np}(\text{BH}_3\text{CH}_3)_4:\text{Zr}(\text{BH}_3\text{CH}_3)_4$	1869	4
$\text{Np}^{4+}:\text{ZrSiO}_4$	1834	This work

Table V. Final parameter values of  $\text{Np}^{4+} : \text{ZrSiO}_4$  (all parameters in  $\text{cm}^{-1}$ )

---

$F^2$	47479(221)
$F^4$	41455(442)
$F^6$	26528(353)
$\alpha$	392(1.9)
$\beta$	-611(76)
$\gamma$	[1200] <sup>a</sup>
$T^2$	[278]
$T^3$	[44]
$T^4$	[64]
$T^6$	[-361]
$T^7$	[434]
$T^8$	[353]
$\zeta$	2088(4)
$M^0$	[0.88]
$M^2$	[0.49]
$M^4$	[0.34]
$P^2$	[500]
$P^4$	[500]
$P^6$	[500]
$B_0^2$	-2537(101)
$B_0^4$	2304(208)
$B_4^4$	-5281(149)
$B_0^6$	-5065(150)
$B_4^6$	642(125)
$n^b$	31 (44)

$\sigma^c$ 

33 {103}

---

<sup>a</sup> Values of the parameters in [ ] are fixed as in Reference 4.

<sup>b</sup> n is the no. of levels; values in { } are for 44 assigned levels with the above parameters.

<sup>c</sup>  $\sigma = \left( \frac{\sum (E_{\text{calc}} - E_{\text{exp}})^2}{n-p} \right)^{1/2}$  where  $E_{\text{calc}}$  and  $E_{\text{exp}}$  are the calculated and experimental energies and p is the number of free parameters.

Table VI. Calculated and experimental energy levels

$\Gamma$	$E_{\text{calc}}$ ( $\text{cm}^{-1}$ )	$E_{\text{obs}}$ ( $\text{cm}^{-1}$ )	$\Delta E$ ( $\text{cm}^{-1}$ )	Eigenvector
6	0	0	0	84.1% $^4I_{9/2}$ + 11.7% $^2H(2)_{9/2}$
6	363.8	350.0	13.8	79.8% $I_{9/2}$ + 13.3% $^2H(2)_{9/2}$
7	557.8			80.1% $^4I_{9/2}$ + 13.4% $^2H(2)_{9/2}$
6	831.1			78.6% $^4I_{9/2}$ + 14.5% $^2H(2)_{9/2}$
7	1374.5			76.7% $^4I_{9/2}$ + 16.9% $^2H(2)_{9/2}$
7	5500.1	5514.0	-13.9	80.4% $^4I_{11/2}$ + 6.9% $^4F_{3/2}$
6	5704.3	5723.0	-18.7	92.2% $^4I_{11/2}$ + 3.3% $^8H(2)_{11/2}$
6	6066.9	6056.0	10.9	88.2% $^4I_{11/2}$ + 4.1% $^2H(2)_{11/2}$
7	6067.7	6072.0	-4.3	85.8% $^4I_{11/2}$ + 3.8% $^2H(2)_{11/2}$
6	6466.5	6468.0	-1.5	88.5% $^4H_{11/2}$ + 4.1% $^2H(2)_{11/2}$
7	6496.3	6496.0	0.3	89.2% $^4I_{11/2}$ + 4.6% $^2H(2)_{11/2}$
7	8286.0	8310.0	-24.0	44.8% $^4F_{3/2}$ + 16.5% $^2D(1)_{3/2}$
6	8408.7	8366.0	42.7	55.5% $^4F_{3/2}$ + 21.0% $^2D(1)_{3/2}$
6	10060.0	10016.0	44.0	80.9% $^4I_{13/2}$ + 5.3% $^2K_{13/2}$
7	10070.4	10062.0	8.4	74.5% $^4I_{13/2}$ + 5.8% $^2K_{13/2}$
7	10529.0	10450.0	79.0*	78.1% $^4I_{13/2}$ + 4.5% $^2K_{13/2}$
7	10583.9			70.0% $^4I_{13/2}$ + 11.4% $^4F_{5/2}$
6	10748.0			66.6% $^4I_{13/2}$ + 5.8% $^4F_{9/2}$
7	11035.3	10896.0	139.3*	66.4% $^4I_{13/2}$ + 6.7% $^4F_{5/2}$
6	11231.7	11147.0	84.7*	28.5% $^4I_{13/2}$ + 11.0% $^4F_{5/2}$
6	11299.7	11571.0	-271.3*	73.1% $^4I_{13/2}$ + 9.0% $^4F_{5/2}$
7	11315.3			12.5% $^4I_{13/2}$ + 11.7% $^2H(2)_{9/2}$
6	11891.8	11935.0	-43.2	21.3% $^4F_{5/2}$ + 15.5% $^2G(1)_{9/2}$

7	11940.6			19.5% ${}^2\text{H}(2)_{9/2}$ + 14.6% ${}^2\text{G}(1)_{9/2}$
7	12211.6	12196.0	15.6	34.6% ${}^4\text{F}_{5/2}$ + 15.9% ${}^4\text{G}_{5/2}$
7	12334.4			45.8% ${}^4\text{F}_{5/2}$ + 8.6% ${}^4\text{I}_{13/2}$
6	12367.6			23.6% ${}^4\text{F}_{5/2}$ + 15.0% ${}^4\text{G}_{5/2}$
6	12569.6	12537.0	32.6	29.7% ${}^2\text{H}(2)_{9/2}$ + 18.0% ${}^2\text{G}(1)_{9/2}$
7	13010.2			63.7% ${}^4\text{G}_{5/2}$ + 7.8% ${}^4\text{F}_{3/2}$
6	13158.2	13188.0	-29.8	36.5% ${}^4\text{S}_{3/2}$ + 17.5% ${}^4\text{I}_{15/2}$
7	13362.0	13352.0	10.0	22.4% ${}^4\text{S}_{3/2}$ + 16.9% ${}^4\text{F}_{5/2}$
6	13594.1			30.3% ${}^4\text{F}_{7/2}$ + 13.1% ${}^4\text{F}_{5/2}$
7	14027.4	13861.0	166.4*	24.3% ${}^4\text{F}_{7/2}$ + 7.9% ${}^4\text{F}_{5/2}$
6	14296.8	14036.0	260.8*	42.6% ${}^4\text{F}_{15/2}$ + 20.0% ${}^4\text{S}_{3/2}$
7	14326.2	14158.0	168.2*	60.2% ${}^4\text{I}_{15/2}$ + 12.7% ${}^2\text{K}_{15/2}$
6	14429.0			26.7% ${}^4\text{G}_{5/2}$ + 16.7% ${}^4\text{F}_{5/2}$
7	14598.4	14555.0	43.4	65.9% ${}^4\text{I}_{15/2}$ + 10.2% ${}^2\text{K}_{15/2}$
7	14865.7			25.7% ${}^4\text{F}_{7/2}$ + 19.4% ${}^4\text{I}_{15/2}$
6	14901.3			37.3% ${}^4\text{F}_{7/2}$ + 22.2% ${}^4\text{G}_{5/2}$
7	14997.4	15014.0	-16.6	29.0% ${}^4\text{I}_{15/2}$ + 23.5% ${}^4\text{G}_{5/2}$
7	15286.8			37.9% ${}^4\text{I}_{15/2}$ + 23.3% ${}^4\text{F}_{7/2}$
6	15578.8			64.8% ${}^4\text{I}_{15/2}$ + 9.5% ${}^2\text{K}_{15/2}$
7	15636.4	15983.0	-346.6*	60.0% ${}^4\text{I}_{15/2}$ + 15.5% ${}^2\text{K}_{15/2}$
6	15697.8			67.6% ${}^4\text{I}_{15/2}$ + 13.0% ${}^2\text{K}_{15/2}$
6	15872.1	16025.0	-138.9*	53.4% ${}^4\text{I}_{15/2}$ + 12.1% ${}^2\text{K}_{15/2}$
7	16466.8	16495.0	-28.2	60.6% ${}^4\text{G}_{7/2}$ + 11.5% ${}^4\text{F}_{7/2}$
6	16542.7	16640.0	97.3*	55.2% ${}^4\text{G}_{7/2}$ + 9.0% ${}^4\text{F}_{7/2}$
7	17002.0			57.7% ${}^4\text{G}_{7/2}$ + 14.9% ${}^4\text{F}_{7/2}$
6	17227.0			55.2% ${}^4\text{G}_{7/2}$ + 19.1% ${}^4\text{F}_{7/2}$

16	17814.4	17869.0	-54.6*	43.6% ${}^4F_{3/2}$ + 12.3% ${}^2H(2)_{9/2}$
7	17962.8			43.0% ${}^4F_{9/2}$ + 11.4% ${}^2H(2)_{9/2}$
6	18207.0			42.0% ${}^4F_{9/2}$ + 17.7% ${}^2H(2)_{9/2}$
6	18436.1	18410.0	26.1	26.0% ${}^4F_{9/2}$ + 23.1% ${}^2K_{13/2}$
7	18778.9			21.4% ${}^2K_{13/2}$ + 18.1% ${}^2H(2)_{11/2}$
7	18805.8			26.9% ${}^2K_{13/2}$ + 19.5% ${}^4F_{9/2}$
6	18832.7			32.0% ${}^2H(2)_{11/2}$ + 18.3% ${}^4G_{11/2}$
6	19002.2	19045.0	-42.8	21.6% ${}^4F_{9/2}$ + 13.3% ${}^2H(2)_{11/2}$
7	19021.5			31.4% ${}^2K_{13/2}$ + 23.2% ${}^4F_{9/2}$
6	19173.6			30.2% ${}^2K_{13/2}$ + 15.4% ${}^4F_{9/2}$
7	19485.0	19350.0	135.0*	27.3% ${}^2H(2)_{11/2}$ + 22.5% ${}^2K_{13/2}$
6	19542.8	19630.0	-87.2*	22.2% ${}^2H(2)_{11/2}$ + 20.5% ${}^2K_{13/2}$
7	19874.8	19895.0	-20.2	51.6% ${}^2H(2)_{11/2}$ + 19.7% ${}^4G_{11/2}$
6	19908.4	19930.0	-21.6	39.4% ${}^2H(2)_{11/2}$ + 17.1% ${}^4G_{11/2}$
6	20028.8			15.1% ${}^2K_{13/2}$ + 13.8% ${}^2H(2)_{11/2}$
7	20063.5			37.0% ${}^2K_{13/2}$ + 19.8% ${}^2H(2)_{11/2}$
7	20162.3			26.7% ${}^2K_{13/2}$ + 7.7% ${}^4S_{3/2}$
7	20382.7			30.7% ${}^2H(2)_{11/2}$ + 22.7% ${}^2K_{13/2}$
6	20513.3	20470.0	43.3	20.5% ${}^4D_{1/2}$ + 17.2% ${}^2P_{1/2}$
7	20537.0			58.7% ${}^2K_{13/2}$ + 8.3% ${}^2G(1)_{7/2}$
6	20808.4			49.0% ${}^2K_{13/2}$ + 9.3% ${}^4G_{9/2}$
7	20852.3			48.7% ${}^4G_{9/2}$ + 11.3% ${}^4D_{5/2}$
6	20970.8			26.2% ${}^4G_{9/2}$ + 14.1% ${}^2P_{1/2}$
6	21203.8			45.7% ${}^4G_{9/2}$ + 7.8% ${}^4D_{5/2}$
6	21369.7			29.0% ${}^4G_{9/2}$ + 10.0% ${}^4D_{5/2}$
7	21422.8			55.4% ${}^4G_{9/2}$ + 6.5% ${}^2H(1)_{9/2}$

6	21714.0	21728.0	-14.0	$34.8\% \ ^4G_{9/2} + 15.9\% \ ^2G(1)_{7/2}$
7	21830.7	21847.0	-16.3	$33.7\% \ ^4D_{5/2} + 20.2\% \ ^2D(2)_{5/2}$
7	21873.5			$28.1\% \ ^2K_{13/2} + 15.2\% \ ^2G(1)_{7/2}$
6	22084.2			$26.3\% \ ^4G_{9/2} + 12.0\% \ ^2G(1)_{7/2}$
7	22289.9			$30.8\% \ ^2K_{13/2} + 15.9\% \ ^2G(1)_{7/2}$
6	22451.8			$29.4\% \ ^4G_{9/2} + 16.9\% \ ^4D_{5/2}$
7	22595.8	22567.0	28.8	$21.1\% \ ^4D_{5/2} + 17.0\% \ ^2D(2)_{5/2}$
6	23106.8			$22.0\% \ ^2K_{15/2} + 16.8\% \ ^2L_{15/2}$
7	23130.2	23100.0	30.2	$22.8\% \ ^2K_{15/2} + 19.0\% \ ^2L_{15/2}$
7	23280.5			$29.2\% \ ^2L_{15/2} + 27.3\% \ ^2K_{15/2}$
6	23734.6			$25.9\% \ ^2L_{15/2} + 18.6\% \ ^2K_{15/2}$
7	23772.2	23760.0	12.2	$20.9\% \ ^4D_{3/2} + 12.0\% \ ^2D(1)_{3/2}$
7	23888.6	23930.0	-41.4	$24.1\% \ ^2K_{15/2} + 18.4\% \ ^2L_{15/2}$
6	23900.7			$22.2\% \ ^2H(1)_{11/2} + 13.8\% \ ^2L_{15/2}$
6	24101.4			$19.3\% \ ^2L_{15/2} + 17.4\% \ ^2K_{15/2}$
6	24331.7			$17.2\% \ ^4D_{3/2} + 13.9\% \ ^2K_{15/2}$
7	24406.9			$24.6\% \ ^2H(1)_{11/2} + 11.7\% \ ^2D(1)_{5/2}$
6	24652.3			$37.7\% \ ^2H(1)_{11/2} + 12.4\% \ ^2I_{11/2}$
7	24672.6			$15.4\% \ ^2D(1)_{5/2} + 13.6\% \ ^2K_{15/2}$
7	24715.0			$25.6\% \ ^2K_{15/2} + 17.4\% \ ^2L_{15/2}$
6	24827.3			$35.1\% \ ^2K_{15/2} + 25.3\% \ ^2L_{15/2}$
6	24921.3			$43.3\% \ ^2H(1)_{11/2} + 22.7\% \ ^4G_{11/2}$
7	25005.4			$52.9\% \ ^2D(1)_{5/2} + 13.2\% \ ^2H(1)_{11/2}$
7	25205.1			$36.8\% \ ^2H(1)_{11/2} + 17.6\% \ ^4G_{11/2}$
6	25893.4			$21.8\% \ ^4G_{11/2} + 14.1\% \ ^2D(1)_{5/2}$

---



\*These thirteen levels were assigned but were not used in the fitting procedure. See text.

Table VII. Comparison of  $U^{4+}$  and  $Np^{4+}$  parameters in different silicates.

	$U^{4+}:\text{ThSiO}_4^a$	$U^{4+}:\text{ZrSiO}_4^b$	$Np^{4+}:\text{ThSiO}_4^{c,d}$	$Np^{4+}:\text{ZrSiO}_4^d$
$F^2 e$	43110(245)	44258	45196(716)	47479[221]
$F^4 e$	40929(199)	40293	38032(546)	41455[442]
$F^6 e$	23834(639)	31287	28343(791)	26528[353]
$\zeta e$	1840(2)	1740	2129(7)	2088[4]
$\alpha e$	32.3(0.4)	23	15(3)	39.2[1.9]
$\beta e$	-663(144)		[-600]	-610(76)
$\gamma e$	[1200]		[1200]	[1200]
$B_0^2 e$	-1003(127)	-2000	323(185)	-2537(101)
$B_0^4 e$	1147(281)	2000	1511(278)	2304(208)
$B_4^4 e$	-2698(251)	-5125	-3559(163)	-5281(149)
$B_0^6 e$	-2889(557)	-5792	-1871(372)	-5065(150)
$B_4^6 e$	-208(333)	427	-801(197)	642(125)
$n$	25	30	29	31 (44)
$\sigma e$	71	112	47	34 (103)
$\frac{F_{\text{cry}}^2}{F_{\text{FI}}^2}$	0.83	0.85	0.83	0.87
$\frac{\zeta_{\text{cry}}}{\zeta_{\text{FI}}}$	0.93	0.88	0.94	0.93
$\frac{F_{\text{cry}}^4}{F_{\text{cry}}^2}$	0.95	0.91	0.84	0.87

$\frac{N_v^e}{(4\pi)^{1/2}}$	1617	3113	1859	-3179
------------------------------	------	------	------	-------

---

<sup>a</sup>Ref. 14

<sup>b</sup>Ref. 13

<sup>c</sup>Ref. 5

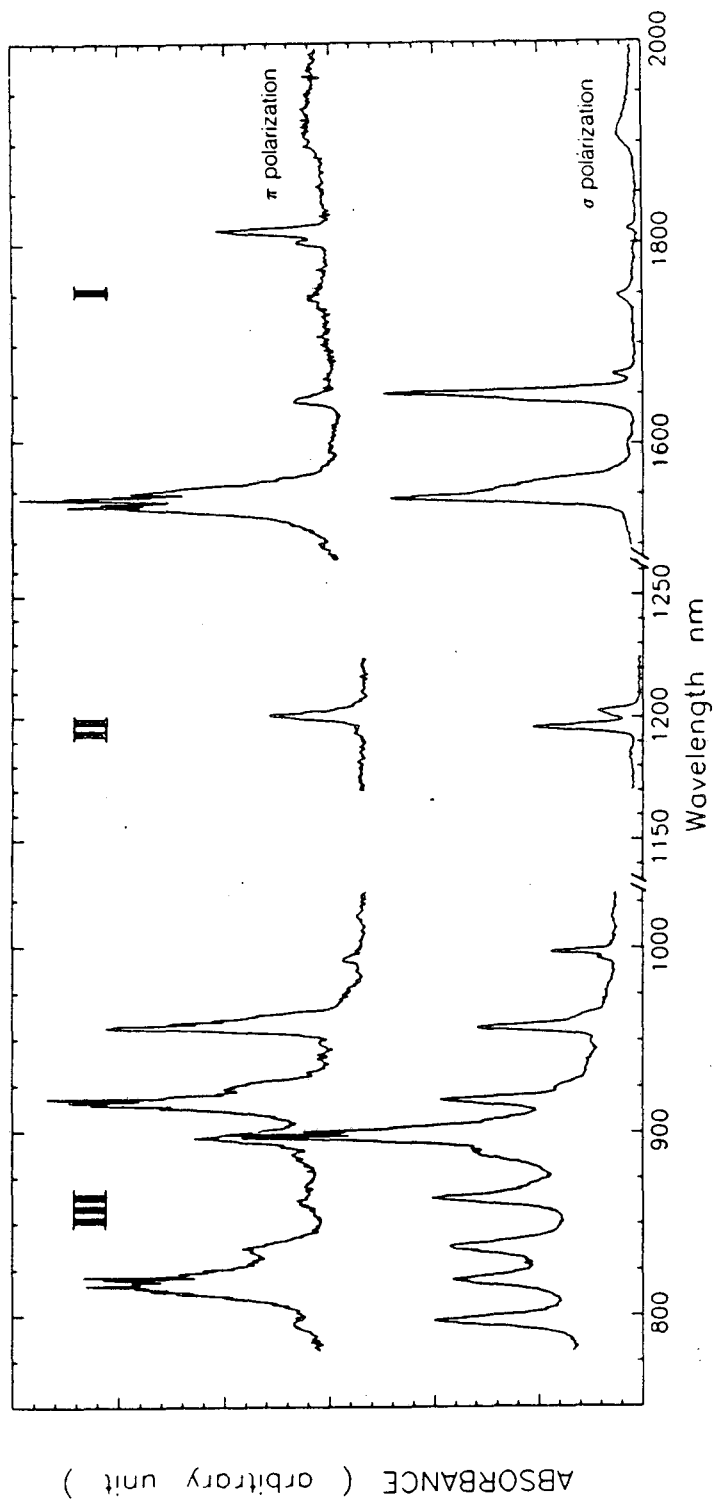
<sup>d</sup>The  $T^k$ ,  $M^k$ , and  $P^k$  values are given in Table V.

<sup>e</sup>in  $\text{cm}^{-1}$ .

## Figure Captions

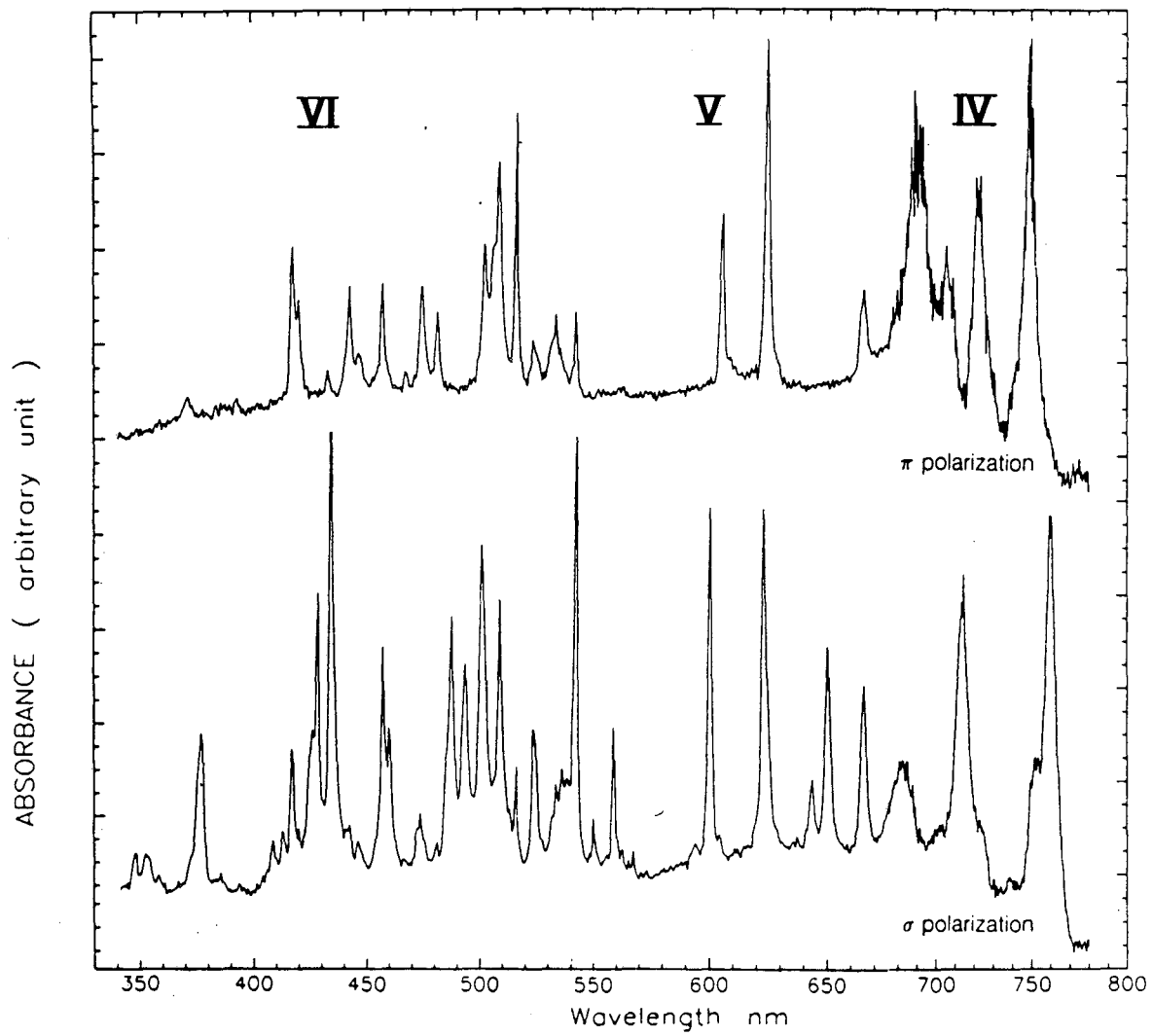
Figure 1. Polarized absorption spectra of the 1 wt %  $\text{Np}^{4+}:\text{ZrSiO}_4$  at 4.2K in the 20000-7800 Å (2000-780 nm) range.

Figure 2. Polarized absorption spectra of the 1 wt %  $\text{Np}^{4+}:\text{ZrSiO}_4$  in the 7800-3400 Å (780-340 nm) range.



XBL 875-2412

Figure 1



XBL 875-2413

Figure 2

*LAWRENCE BERKELEY LABORATORY  
TECHNICAL INFORMATION DEPARTMENT  
UNIVERSITY OF CALIFORNIA  
BERKELEY, CALIFORNIA 94720*